


## Research Paper

# Investigation on the mass transferring near-contact binary TT Cet

Xiao-Man Tian<sup>1,2</sup>  and Lin-Feng Chang<sup>3,4,5</sup>

<sup>1</sup>School of Aeronautics, Shandong Jiaotong University, 5001 Haitang Road, Changqing District, 250000 Jinan, China, <sup>2</sup>Center for Astronomical Mega-Science, Chinese Academy of Sciences, 20A Datun Road, Chaoyang District, 100012 Beijing, China, <sup>3</sup>Yunnan Observatories, Chinese Academy of Sciences (CAS), P. O. Box 110, 650216 Kunming, China, <sup>4</sup>Key Laboratory of the Structure and Evolution of Celestial Objects, Chinese Academy of Sciences, P. O. Box 110, 650216 Kunming, China and <sup>5</sup>University of the Chinese Academy of Science, Yuquan Road 19, Sijingshang Block, 100049 Beijing, China

### Abstract

First multi-colour complete light curves and low-resolution spectra of short-period eclipsing binary TT Cet are presented. The stellar atmospheric parameters of the primary star were derived through spectra fitting as:  $T_{\text{eff}} = 7\,091 \pm 124$  K,  $\log g = 4.15 \pm 0.33$  cm/s<sup>2</sup>, and  $[Fe/H] = -0.23 \pm 0.04$  dex. The light curves were analysed using the Wilson–Devinney code. The photometric solution suggests that this target should be a near-contact binary with the primary component filling its critical Roche lobe (i.e. SD1-type NCB). The luminosity enhancement around the primary light maximum (phase 0.10–0.40) on the light curve was detected like other SD1-type NCBs, which could be caused by a hot spot near the facing surface of the secondary component due to mass transfer. Long-term decrease of the orbital period at a rate of  $dP/dt = -5.01 (\pm 0.06) \times 10^{-8}$  d · yr<sup>-1</sup> was detected by the O–C analysis, which supports the mass transfer from the primary to the secondary and is consistent with its primary filling configuration. No third body was found through the light curve and O–C analysis. TT Cet may locate in the broken contact stage predicted by the thermal relaxation oscillation theory (TRO) and will evolve to the contact stage eventually. It is another good observational example supporting the TRO theory. We have collected all known SD1-type NCBs with absolute parameters from the literatures. The relations of these parameters are summarised for these rare systems.

**Keywords:** stars: binaries: close – stars: binaries: eclipsing – stars: binaries: individual (TT Cet) – stars: evolution

(Received 16 March 2020; revised 4 June 2020; accepted 9 June 2020)

## 1. Introduction

Near-contact binaries (NCBs) are eclipsing binaries that show following characteristics commonly: continuous EB-type light variations, facing surface less than 0.1 orbital radius apart, short period (less than 1 d), and one or two components at or near their Roche lobes (Shaw 1994). According to their geometric structure, NCBs can be classified into following sub-classes: semi-detached systems with one component filling its critical Roche lobe (including SD1 and SD2 types, which represent systems with primaries and secondaries filling their critical Roche lobes, respectively), marginal contact, and marginal detached systems (Zhu & Qian 2009). Mass transfer occurs in such binaries frequently. NCBs have been the significant transition targets between tidal-locked detached systems and W UMa-type overcontact systems.

TT Cet was confirmed as one  $\beta$  Lyrae candidate system by Hoffman et al. (2008), and the light curve showed EB-type characteristic (Deb & Singh 2011). Brancewicz & Dworak (1980) obtained the geometric and physical parameters of this target using the iterative method. Duerbeck & Rucinski (2007) acquired the preliminary orbit parameters through the radial velocity (RV) measurement. According to their investigation, the mass ratio was determined as  $q_{sp} = 0.39 \pm 0.07$ , and the spectral type of the primary star was estimated as F4 V. Then Pribulla et al. (2009) measured the RVs of both components and confirmed

a same spectra type for primary star as Duerbeck & Rucinski (2007). Using the photometric and spectroscopic data of All Sky Automated Survey-3 project, new estimation of physical and absolute parameters (including a updated period of 0.485952 d) were made by Deb & Singh (2011). TT Cet was marked as a contact binary in the catalogue of Giuricin, Mardirossian, & Mezzetti (1983) and as a near-contact binary (NCB) in the catalogue of Shaw (1994). Duerbeck & Rucinski (2007) found that TT Cet might be a detached system rather than a semi-detached system with a quite faint and cool secondary component.

In this study, the first multi-colour high-precision light curves, low-resolution spectrum, and O–C diagram were acquired. The detailed light curve analysis, spectra fitting, and period investigation were presented. We also collected all known SD1-type NCBs with absolute parameters from the literatures. The relations of these parameters are summarised for these rare systems.

## 2. Observation and data reduction

### 2.1. Photometric observations

New light curve in Cousin  $I_c$  band (Bessell 1983) was observed on 2005 November 29, December 7, and 2006 February 3 with the Andor DW436 2K Charge Coupled Device (CCD) camera mounted on the 1-m telescope (labelled as ‘D1 m’) at Yunnan Observatories (YNO), Chinese Academy of Sciences (CAS). The first multi-colour light curves of this target in Johnson–Cousin  $BVR_cI_c$  filters (Ažusienis & Straižys 1969; Bessell 1983) were observed with the Andor DW936 2K CCD camera mounted on

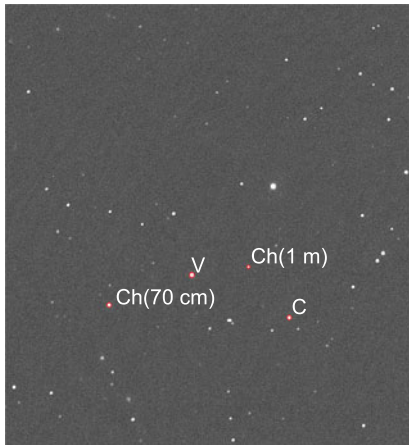
**Author for correspondence:** Xiao-Man Tian, E-mail: txmjlx2018@163.com

**Cite this article:** Tian X-M and Chang L-F. (2020) Investigation on the mass transferring near-contact binary TT Cet. *Publications of the Astronomical Society of Australia* 37, e031, 1–12. <https://doi.org/10.1017/pasa.2020.22>

© Astronomical Society of Australia 2020; published by Cambridge University Press

**Table 1.** Photometric observation Log of TT Cet

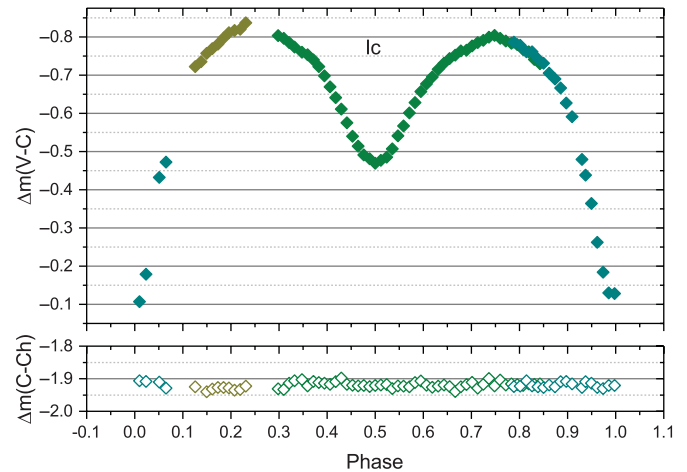
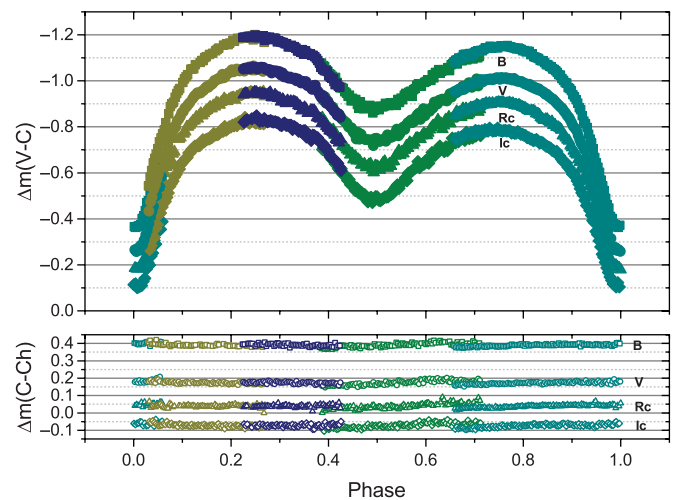
Data	Filter	Telescopes	Field
2005 Nov 29	$I_c$	1 m	$7.3' \times 7.3'$
2005 Dec 7	$I_c$	1 m	$7.3' \times 7.3'$
2006 Feb 3	$I_c$	1 m	$7.3' \times 7.3'$
2018 Dec 25	$BVR_cI_c$	70 cm	$20' \times 20'$
2018 Dec 31	$BVR_cI_c$	70 cm	$20' \times 20'$
2019 Jan 24	$BVR_cI_c$	70 cm	$20' \times 20'$
2019 Jan 27	$BVR_cI_c$	70 cm	$20' \times 20'$

**Figure 1.** Observed CCD image of TT Cet. ‘Variable star’, ‘Comparison star’ are marked with ‘V’ and ‘C’, respectively. Ch(1 m) and Ch(70 cm) represent the corresponding check stars for light curves observed with ‘D1 m’ and ‘D70 cm’, respectively.

the 70-cm Sino-Thai telescope (labelled as ‘D70 cm’) locating at Lijiang Observing Station of YNO on 2018 December 25, 31 and 2019 January 24, 27. The detailed observation log is given in Table 1. PHOT package of IRAF was used to process all observation images.

In order to distinguish the two sets of light curves, the light curve in the  $I_c$  band observed with 1-m telescope and light curves in the  $BVR_cI_c$  band obtained with 70-cm telescope are labelled as ‘ $LC_{D1\text{ m}}$ ’ and ‘ $LC_{D70\text{ cm}}$ ’, respectively. The nearby invariable comparison star and check stars were chosen to determine the differential magnitudes. TYC 5278-951-1 was chosen as comparison star for the two sets of light curves. Because the field of views of the two telescopes are different, TYC 5277-893-1 and Gaia DR2 2464167327789832960 (Gaia Collaboration et al. 2018) ( $\alpha_{2000} = 01^{\text{h}}47^{\text{m}}08^{\text{s}}.34$ ,  $\delta_{2000} = -09^{\circ}45'14''.50$ ), were chosen as check stars for light curves  $LC_{D1\text{ m}}$  and  $LC_{D70\text{ cm}}$ , respectively. The information of comparison and check stars along with the target TT Cet are listed in Table 2. In the table, the V band magnitudes were taken from the Tycho-2 Catalog (Høg et al. 2000) and the G band magnitude of the check star  $Check(Ch)_{LC_{1\text{ m}}}$  was acquired from the Gaia DR2 data (Gaia Collaboration et al. 2018). The  $B-V$  colour indices of the variable star and comparison star are 0.44 and 0.56 (Høg et al. 2000), respectively.

One observation image is shown in Figure 1. In the figure, variable star is marked with ‘V’, comparison star is marked with ‘C’, and check stars are marked with Ch(1 m) and Ch(70 cm), respectively. The light curves observed with telescope ‘D1 m’ and ‘D70 cm’ are shown in Figures 2 and 3, respectively. Different colours represent the data observed on different night. The square,

**Figure 2.** Light curve of TT Cet on the  $I_c$  band observed by ‘D1 m’.**Figure 3.** Light curves of TT Cet on  $BVR_cI_c$  bands observed by ‘D70 cm’.

circle, triangle, and rhombus signs show the B, V,  $R_c$ , and  $I_c$  band data, respectively. The magnitude difference of the comparison star and check star are shown in the bottom of the figures. The standard deviation of magnitude difference is about 0.009, 0.01 in the  $LC_{D1\text{ m}}$  and  $LC_{D70\text{ cm}}$ , respectively. In Figures 2 and 3, one can see that the light curves are asymmetry, which show obvious O’Connell effect. Take the  $LC_{D70\text{ cm}}$ , for example, the luminosity difference (i.e. Max.I–Max.II) of  $BVR_cI_c$  bands are about 0.049, 0.046, 0.044, and 0.040 mag, respectively. And Max.I and Max.II are the maximum brightness at 0.25 and 0.75 phase of the light curve from the primary eclipse, respectively. We note that the luminosity differences of short-wavelength bands are larger than those of long-wavelength bands (i.e. short-wavelength bands are more sensitive to the perturbation causing O’Connell phenomenon than long-wavelength bands).

## 2.2. Spectra observation

The spectra observation was performed on 2018 September 30 with the Beijing Faint Object Spectrograph and Camera

**Table 2.** Information of TT Cet and the corresponding comparison and check stars

Targets	Name	$\alpha_{2000}$	$\delta_{2000}$	Mag
Variable (V)	TT Cet	01 <sup>h</sup> 46 <sup>m</sup> 56 <sup>s</sup> .50	−09°45′09″.75	V = 10.91
Comparison (C)	TYC 5278-951-1	01 <sup>h</sup> 47 <sup>m</sup> 15 <sup>s</sup> .76	−09°42′30″.97	V = 11.89
Check(Ch) <sub>LC70cm</sub>	TYC 5277-893-1	01 <sup>h</sup> 46 <sup>m</sup> 38 <sup>s</sup> .93	−09°44′07″.23	V = 12.03
Check(Ch) <sub>LC1m</sub>		01 <sup>h</sup> 47 <sup>m</sup> 08 <sup>s</sup> .34	−09°45′14″.50	G = 14.07

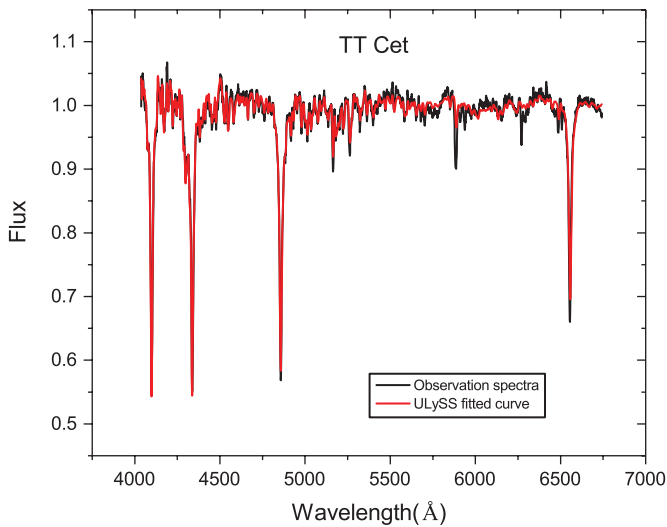


**Figure 4.** Spectrum of TT Cet observed on 2018 September 30. The black and red lines in the top panel represent the observed and fitted spectrum, respectively.

(BFOSC) mounted on the 2.16-m telescope of Xinglong station of National Astronomical Observatories of China (NAOC), CAS. Low-dispersion spectrometer BFOSC and grism G7 were used. The slit width and the line dispersion of grism G7 are 1.8 arcsec and 95 Åmm<sup>−1</sup>, respectively. The observation wavelength range is 400–680nm (Fan et al. 2016). IRAF was used to process the observation images and extract the spectra. Normalised flux was obtained and the atmospheric absorption lines were corrected. Because of the low resolution, the observed spectrum can only show the spectral lines of the primary star, and the lines of the secondary star may be too faint to be detected. The observed spectrum is shown in Figure 4 with black line. University of Lyon Spectroscopic analysis Software (ULySS) (Koleva et al. 2009) was employed to acquire the atmospheric parameters through full spectra fitting with model spectra generated by an interpolator with the ELODIE library (Prugniel & Soubiran 2001). The red line in the Figure 4 shows the fitted spectrum. The stellar atmospheric parameters of the primary star of TT Cet were derived as:  $T_{eff} = 7091 \pm 124$  K,  $\log g = 4.15 \pm 0.33$  cm/s<sup>2</sup>,  $[Fe/H] = -0.23 \pm 0.04$  dex. The same method was used to analyse the data from the Large Sky Area Multi-Object Fiber Spectroscopic Telescope spectroscopic survey, and stellar atmospheric parameters of many binary systems were derived (Qian et al. 2017, 2018, 2019). Because the secondary star is quite faint and the primary star contributes the most light to the total system, the atmospheric parameters obtained by ULYSS can be used to describe the atmospheric characteristic of the primary star. The temperature of the primary star can be adopted as 7091 K. The comparisons of our calibrated spectrum with three standard spectra from the Sloan Digital Sky Survey (SDSS) (Vanden Berk et al. 2001) are shown

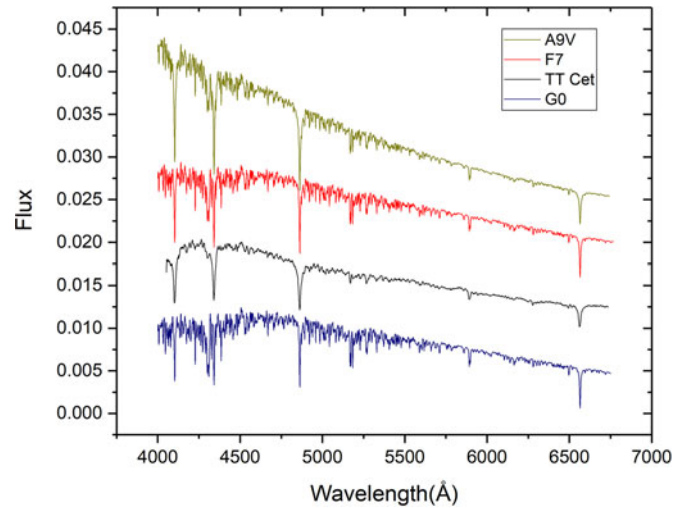


**Figure 5.** Calibrated spectrum of TT Cet and the A9V, F7, G0 standard spectra from SDSS (Vanden Berk et al. 2001)

in Figure 5. From the figure, we can see that the primary component should be a F7-type star, which is agreed well with its colour ( $B - V = 0.44$ ) (Cox & Pilachowski 2000).

### 3. O–C diagram analyses

We collected all available times of light minimum with error. Combined with four eclipse times observed by us, totally 92 eclipse times crossing about 50 yr were used to construct the O–C diagram. All eclipse times with available error used for the period analysis are listed in Table 3, in which *P* and *S* marked the primary and secondary eclipse times, respectively. The *O–C gateway* in the reference column means that the data were collected from the O–C gateway web and the original publications are unavailable on line. The corresponding O–C and cycle *E* were computed with follow ephemeris.

$$MinI = HJD2458484.16341 + 0.485952^d \times E. \tag{1}$$

The O–C diagram of TT Cet is plotted in Figure 6 with error bars, in which the cross, triangle, and circle dot signs represent the data obtained with visual (vis), photoelectricity (Pe), and CCD-type detectors, respectively. A weight of 1 for vis data and a high weight of 5 for Pe and CCD data were applied in the O–C analysis. Based on the least-squares method, the following equation can be used to describe the O–C diagram:

$$MinI = HJD 2458484.16134(.00009) \tag{2}$$

$$+ 0.485953(\pm 0.001321) \times E \tag{3}$$

$$- 3.33(\pm 0.04) \times 10^{-11} \times E^2. \tag{4}$$

**Table 3.** Times of light minima of TT Cet

HJD(2400000+)	Error	Min.	Meth.	E	O-C(d)	References
40119.46100		P	vis	-37 791	-0.09038	Diethelm et al. (1974a)
40152.50800		P	vis	-37 723	-0.08811	Diethelm et al. (1974a)
40157.37100		P	vis	-37 713	-0.08463	Diethelm et al. (1974a)
40181.40600		S	vis	-37 663.5	-0.10426	Diethelm et al. (1974a)
40205.24000		S	vis	-37 614.5	-0.08191	Diethelm et al. (1974a)
40220.30700		S	vis	-37 583.5	-0.07942	Diethelm et al. (1974)
40221.26600		S	vis	-37 581.5	-0.09232	Diethelm et al. (1974)
40238.27900		S	vis	-37 546.5	-0.08764	Diethelm et al. (1974)
40442.61500		P	vis	-37 126	-0.09446	Carnevali et al. (1975)
40501.42100		P	pe	-37 005	-0.08865	Kizilirmak & Pohl (1971)
44457.83830		S	vis	-28 863.5	-0.04956	Wolf & Kern (1983)
44457.84700		S	vis	-28 863.5	-0.04086	Wolf & Kern (1983)
44468.76450		P	vis	-28 841	-0.05728	Wolf & Kern (1983)
46327.54100		P	vis	-25 016	-0.04718	– (1986)
46350.38200		P	vis	-24 969	-0.04592	– (1986)
46401.40200		P	vis	-24 864	-0.05088	– (1986)
46402.37100		P	vis	-24 862	-0.05379	– (1986)
46403.34400		P	vis	-24 860	-0.05269	– (1986)
46707.55400		P	vis	-24 234	-0.04864	– (1987a)
46821.27500		P	vis	-24 000	-0.04041	– (1987b)
47115.26800		P	vis	-23 395	-0.04837	– (1988)
47471.47000		P	vis	-22 662	-0.04919	– (1989)
48500.24460		P	CCD + V	-20 545	-0.03497	O-C gateway
48521.63000	0.00800	P	CCD	-20 501	-0.03146	– (1992a)
48890.45500	0.00800	P	CCD	-19 742	-0.04403	– (1992b)
50446.24710	0.00030	S	CCD	-16 540.5	-0.02725	Agerer & Huebscher (1998)
50702.58700	0.00400	P	CCD	-16 013	-0.02703	– (1998)
50750.45380	0.00040	S	CCD	-15 914.5	-0.02651	Agerer & Hubscher (1999)
51397.98300		P	CCD	-14 582	-0.02835	O-C gateway
51462.13380		P	CCD	-14 450	-0.02321	O-C gateway
51462.13400		P	CCD + R	-14 450	-0.02301	O-C gateway
51869.84500		P	CCD + V	-13 611	-0.02574	O-C gateway
51869.85000		P	CCD + V	-13 611	-0.02074	O-C gateway
51879.32470	0.00060	S	CCD + Ir	-13 591.5	-0.02210	Agerer & Hubscher (2002)
52224.60500		P	vis	-12 881	-0.01070	O-C gateway
52237.96230		S	CCD + R	-12 853.5	-0.01708	O-C gateway
52238.67720		P	CCD	-12 852	-0.03111	O-C gateway
52245.97570		P	CCD	-12 837	-0.02189	O-C gateway
52245.97580		P	CCD + Rc	-12 837	-0.02179	O-C gateway
52581.77020		P	CCD	-12 146	-0.02022	O-C gateway
52582.01510		S	CCD + Ic	-12 145.5	-0.01829	O-C gateway
52638.62720		P	CCD	-12 029	-0.01960	O-C gateway
52999.69090		P	CCD	-11 286	-0.01824	O-C gateway
53271.33940	0.00020	P	CCD + BVR	-10 727	-0.01691	Cakirli et al. (2006)
53271.58390	0.00020	S	CCD + BVR	-10 726.5	-0.01538	Cakirli et al. (2006)
53272.31170	0.00020	P	CCD + BVR	-10 725	-0.01651	Cakirli et al. (2006)

Table 3. Continued

HJD(2400000+)	Error	Min.	Meth.	E	O-C(d)	References
53273.52780	0.00020	S	CCD + BVR	-10 722.5	-0.01529	Cakirli et al. (2006)
53274.50020	0.00020	S	CCD + BVR	-10 720.5	-0.01479	Cakirli et al. (2006)
53275.47140	0.00030	S	CCD + BVR	-10 718.5	-0.01550	Cakirli et al. (2006)
53276.44490	0.00020	S	CCD + BVR	-10 716.5	-0.01390	Cakirli et al. (2006)
53288.83320		P	CCD	-10 691	-0.01738	O-C gateway
53311.66850	0.00100	P	CCD	-10 644	-0.02182	Ogloza et al. (2008)
53316.04510		P	CCD + Rc	-10 635	-0.01879	O-C gateway
53663.01640		P	CCD + Rc	-9 921	-0.01722	O-C gateway
53704.08079	0.00099	S	CCD + Ic	-9 836.5	-0.01577	This study
53712.09653	0.00053	P	CCD + Ic	-9 820	-0.01824	This study
53709.67020		P	CCD	-9 825	-0.01481	O-C gateway
53983.26220		P	CCD + Ic	-9 262	-0.01379	O-C gateway
54054.69680		P	CCD	-9 115	-0.01413	O-C gateway
54091.62930		P	CCD	-9 039	-0.01398	O-C gateway
54380.77440	0.00030	P	CCD	-8 444	-0.01032	Samolyk (2008a)
54419.64730	0.00020	P	CCD	-8 364	-0.01358	Samolyk (2008a)
54449.77680	0.00020	P	CCD	-8 302	-0.01311	Samolyk (2008a)
54708.78940	0.00020	P	CCD	-7 769	-0.01292	Samolyk (2008b)
54713.16190		P	CCD + Rc	-7 760	-0.01399	O-C gateway
54741.10400		S	CCD + Ic	-7 702.5	-0.01413	O-C gateway
54809.38390	0.00060	P	CCD + Ir	-7 562	-0.01049	Hubscher, Steinbach, & Walter (2009)
55102.89830	0.00010	P	CCD + V	-6 958	-0.01109	Diethelm (2010)
55144.68990	0.00010	P	CCD	-6 872	-0.01137	Samolyk (2010)
55486.80040	0.00010	P	CCD + V	-6 168	-0.01107	Samolyk (2011)
55508.66890	0.00010	P	CCD + V	-6 123	-0.01041	Samolyk (2011)
55533.69670	0.00020	S	CCD + V	-6 071.5	-0.00914	Diethelm (2011)
55811.9036	0.00020	P	CCD	-5 499	-0.00976	Samolyk (2012)
55888.684	0.00010	P	CCD	-5 341	-0.00978	Samolyk (2012)
55896.70590	0.00050	S	CCD	-5 324.5	-0.00609	Diethelm (2012)
56247.32000	0.00300	P	CCD	-4 603	-0.00635	Paschke (2013)
56253.63520	0.00010	P	CCD	-4 590	-0.00853	Samolyk (2013a)
56271.61540		P	CCD + V	-4 553	-0.00855	Samolyk (2013b)
56538.88980		P	CCD + V	-4 003	-0.00775	Samolyk (2013b)
56949.03350		P	CCD + Ic	-3 159	-0.00754	O-C gateway
57331.96570		P	CCD + B	-2 371	-0.00552	O-C gateway
57331.96590		P	CCD + V	-2 371	-0.00532	O-C gateway
57331.96680		P	CCD + Ic	-2 371	-0.00442	O-C gateway
57342.65750		P	CCD + V	-2 349	-0.00466	O-C gateway
57358.69460		P	CCD	-2 316	-0.00398	O-C gateway
58067.69780		p	CCD	-857	-0.00475	O-C gateway
58077.9034		P	CCD + V	-836	-0.00414	O-C gateway
58077.90410		P	CCD + Ic	-836	-0.00344	O-C gateway
58083.73570		p	CCD + V	-824	-0.00326	O-C gateway
58136.70620		p	CCD + V	-715	-0.00153	O-C gateway
58478.09057	0.00048	S	CCD + BVRlc	-12.5	0.00156	This study
58484.16341	0.00011	P	CCD + BVRlc	0	0.00000	This study

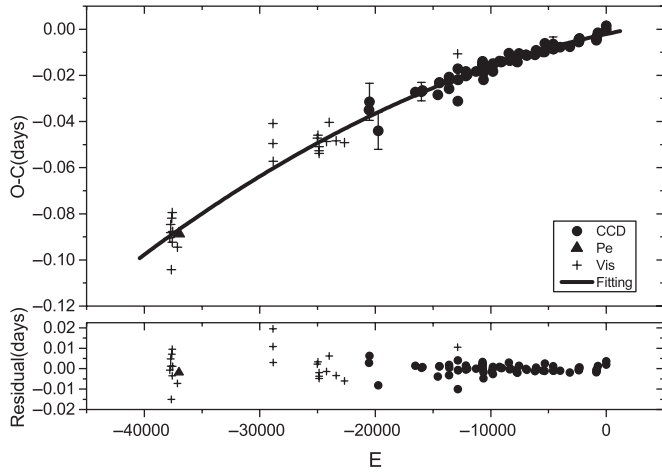


Figure 6. O-C diagram of TT Cet

The quadratic term in the equation signifies that the period is undergoing a long-term decrease at a rate of  $dP/dt = -5.01(\pm 0.06) \times 10^{-8} \text{ d} \cdot \text{yr}^{-1}$ . The fitted curve was plotted in Figure 6 with black line and the residuals were shown in the bottom. There is no other change in the residuals and no third body was detected through our period analysis.

#### 4. Light curve analyses

The multi-colour light curves of TT Cet were obtained for the first time. In order to acquire the phased light curves more accurately, different linear ephemerides were used for two sets of light curves. For the light curve  $LC_{D1m}$ , the following linear ephemeris was used:

$$\text{MinI} = \text{HJD } 2453712.09653(99) + 0.485952^d \times E. \quad (5)$$

While for the light curves  $LC_{D70cm}$ , the following linear ephemeris was used:

$$\text{MinI} = \text{HJD } 2458484.16341(11) + 0.485952^d \times E, \quad (6)$$

in these equations, epoch 2453712.09653(99) and 2458484.16341(11) are the primary eclipse times observed during the corresponding light curve observation.

Wilson-Devinney (W-D) program (Wilson & Devinney 1971; Wilson 1990, 2012) was used to analyse the light curves. During the solution process, the effective temperature of the primary star was fixed at 7091 K, which was estimated from our spectral analysis. The RV data of two components acquired from Duerbeck & Rucinski (2007) and Pribulla et al. (2009) were applied in the WD modelling, which can help to obtain more reliable measurements of the components, such as masses. The phase of the data was recalculated using a more appropriate epoch 2450702.587(4) and a period of 0.475852 d. The gravity-darkening coefficients of the components are adopted as  $g_1 = g_2 = 0.32$ . The bolometric albedos are taken as  $A_1 = A_2 = 0.5$  (Ruciński 1969) according to the convective envelopes ( $T < 7200 \text{ K}$ ) of both components. Meanwhile, the bandpass limb-darkening coefficients [taken from van Hamme (1993)] and the logarithmic bolometric coefficients were applied. As we can see in Figures 2 and 3, the light curves show obvious O'Connell effect with brightness enhancement at the primary light maximum. The asymmetry means that the light curves have been disturbed by some perturbation caused by the

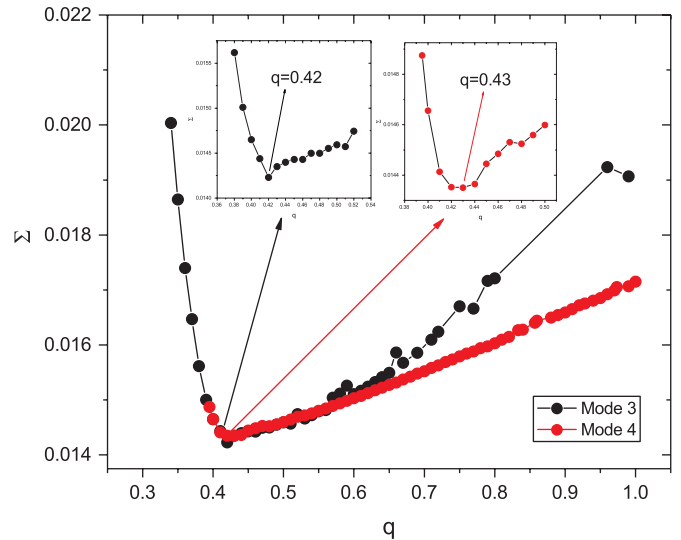


Figure 7.  $\Sigma - q$  curves.

photospheric activity of the component. We note that the short-wavelength bands behaved more sensitive to the perturbation than long-wavelength bands. Moreover, for such late type system, spot model should be more convective to explain the brightness enhancement around phase 0.10–0.40. The convergent solutions with mode 4 (the semi-detached case with the primary component filling the critical Roche lobe) and mode 3 (over contact case) with a hot spot were acquired. Spot model was employed for the light curve fit with four adjustable parameters: the latitude of spot center ( $\theta$ ) in degree; the longitude of spot center ( $\phi$ ) in degree; spot angular radius ( $r$ ) in radian; and the spot temperature factor  $T_f$  ( $T_f = T_s/T_*$ , in which  $T_s$  is the spot temperature and  $T_*$  is the photosphere surface temperature of the star). The adjustable parameters of mode 4 are as follow: the monochromatic luminosity of primary star,  $L_{1B}, L_{1V}, L_{1Rc}, L_{1Ic}$ ; the orbital inclination,  $i$ ; the mean temperature of secondary star,  $T_2$ ; and the dimensionless potential of the secondary star,  $\Omega_2$ . Compared with mode 4, the only one different adjustable parameter of mode 3 is the dimensionless potential of the components  $\Omega_1 = \Omega_2$ . The third light  $L_3$  was adjustable parameter at each mode, but no converged result was obtained. In order to confirm a more reliable mass ratio, the photometric solutions based on a group of assumed mass ratio values from 0.01 to 1 were obtained with the differential correction program. The search step length is 0.01. For all assumed values of  $q$ , the sums of weighted square deviations ( $\sum (O - C)_i^2$ ) with mode 3 and mode 4 are displayed in Figure 7. One can see from this figure, the minimal values achieved at  $q = 0.43$  and  $q = 0.42$  with mode 4 and mode 3, respectively. Then, the mass ratio was made as one adjustable parameter. The theoretical light curves obtained from mode 3 and mode 4 are shown in Figure 8 with green lines and black lines, respectively. The spotted theoretical light curves with both modes fitted the observed light curves very well. The final converged photometric solutions show that the brightness enhancement can be explained by the appearance of a hot spot near the facing surface of the secondary component due to the mass transfer. All converged photometric solutions are listed in Table 4. The uncertainty of mass ratio in the table was given by WD program with the standard method. In addition, the  $q$ -search curve bottom can be used to confirm the uncertainty of

**Table 4.** Spotted photometric solutions of TT Cet

Parameters	Mode 4		Mode 3	
	LC(70 cm)	LC (1 m)	LC (70 cm)	LC (1 m)
$g_1 = g_2$	0.32 (fixed)	0.32 (fixed)	0.32 (fixed)	0.32 (fixed)
$A_1 = A_2$	0.5 (fixed)	0.5 (fixed)	0.5 (fixed)	0.5 (fixed)
$q (M_2/M_1)$	0.430 (4)	0.431 (10)	0.420 (1)	0.415 (2)
$T_1(K)$	7 091	7 091	7 091	7 091
$T_2(K)$	5 414 (10)	5 378 (23)	5 383 (11)	5 353 (23)
$i(^{\circ})$	82.59 (29)	82.85 (52)	82.23 (20)	82.44 (53)
$\Omega_1$	2.739	2.740	2.715 (2)	2.7038 (3)
$\Omega_2$	2.751 (13)	2.760 (35)	2.715	2.7038
$L_1/L_{totalB}$	0.9149 (1)	-	0.9176 (1)	-
$L_1/L_{totalV}$	0.8808 (1)	-	0.8835 (1)	-
$L_1/L_{totalR_c}$	0.8596 (2)	-	0.8622 (2)	-
$L_1/L_{totalI_c}$	0.8382 (3)	0.8430 (4)	0.8407 (2)	0.8450 (3)
$r_1(pole)$	0.427 (1)	0.427 (2)	0.4294 (2)	0.4303 (3)
$r_1(side)$	0.455 (1)	0.455 (2)	0.4579 (3)	0.4590 (5)
$r_1(back)$	0.482 (1)	0.482 (2)	0.4852 (4)	0.4862 (8)
$r_2(pole)$	0.286 (4)	0.285 (10)	0.2868 (8)	0.2857 (9)
$r_2(side)$	0.298 (5)	0.297 (12)	0.2992 (10)	0.2979 (11)
$r_2(back)$	0.329 (8)	0.327 (20)	0.3322 (17)	0.3309 (19)
$R_2/R_1$	0.670 (11)	0.666 (25)	0.6705 (15)	0.6666 (17)
$f(fill - degree)_2$	0.966 (53)	0.95 (12)	-	-
$f$	-	-	0.013 (7)	0.014 (1)
Latitude (degree)	85.81 ( $\pm 11.10$ )	85.81 (fixed)	82.14 ( $\pm 8.38$ )	82.14 (fixed)
Longitude (degree)	100.56 (78)	100.56 (fixed)	100.48 (73)	100.48 (fixed)
Radius (radian)	0.395 (44)	0.395 (fixed)	0.384 (36)	0.384 (fixed)
$T_f(T_s/T_*)$	1.300 (39)	1.300 (fixed)	1.314 (43)	1.314 (fixed)
$\sum(O - C)^2$	0.0135	0.0045	0.0134	0.0045

LC, light curve

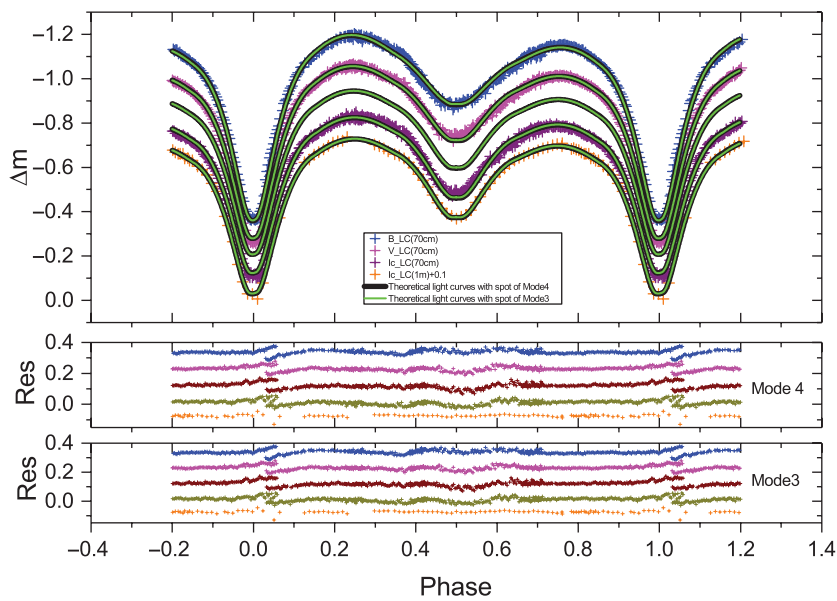


**Figure 8.** The theoretical light curves with hot spot of TT Cet with mode 3 and mode 4.

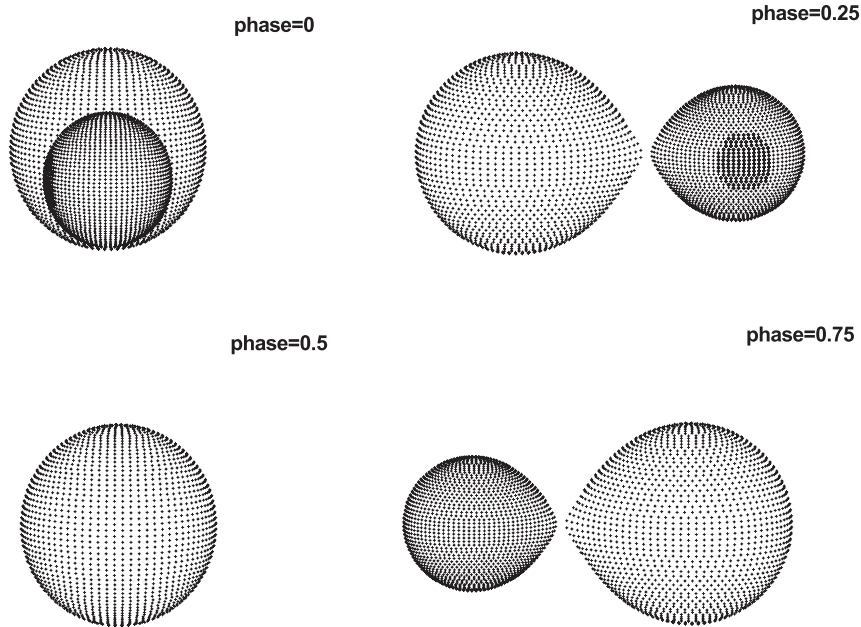


**Figure 9.** Geometrical structure of TT Cet with bolding region marking the position of the hot spot with mode 4.

the mass ratio. It can be seen from Figure 7, the q-search bottom with mode 3 is clearly sharp around 0.420(1), the uncertainty may be 0.01. The q-search bottom with mode 4 is narrow (visually, from 0.42 to 0.44), so the mass ratio 0.430(4) may have an uncertainty of 0.04. The geometric structure in 3D view with mode 4 is shown in Figure 9, and the bolding region shows the position of the hot spot.

## 5. Discussion and conclusion

### 5.1. Investigation on TT Cet

The atmosphere parameters of the primary component obtained from the spectra fit are as follows:  $T_{eff} = 7091 \pm 124$  K,  $\log g = 4.15 \pm 0.33$  cm/s<sup>2</sup>, and  $[Fe/H] = -0.23 \pm 0.04$  dex. The light curves of this target show  $\beta$  Lyrae characteristics. The asymmetrical light curves show obvious O'Connell effect with about 0.05 mag brightness enhancement around the primary light maximum. The spotted theoretical light curves with mode 3 and mode 4 fitted the light curves quite well. The brightness enhancement around phase 0.10–0.40 could be explained by a hot spot near the facing surface of the secondary component causing by the mass transfer from the primary component. The solution with over contact mode shows that the system should be an extremely shallow contact binary with  $f = 0.013(7)$ . Therefore, the semi-detached mode, with the primary component filling its Roche lobe, may be more reasonable than the contact model. TT Cet should be one SD1-type near-contact binary. Such brightness enhancement also appears in other SD1-type NCBs, such as BL And (Zhu & Qian 2006), BS Vul (Zhu et al. 2012), GR Tau (Qian 2002a), and V473 Cas (Zhu et al. 2009). The solutions with semi-detached mode show that the primary component of TT Cet has already filling its Roche lobe and the secondary is nearly filling the Roche lobe with a fill-degree factor  $f(fill - degree)_2 = 0.966(53)$ . The orbital inclination is  $i = 82.59(29)^\circ$ , which means that the system is totally eclipse and the photometric solutions are reliable. The temperature difference

between the components is about 1700 K. TT Cet should consist of a F7-type primary star and a G7-type secondary star (Cox & Pilachowski 2000). The semi-major axis was estimated as  $a = 3.405282R_\odot$  through the WD progress, which can be used to compute the total mass  $M$  of the binary system

$$M = M_1 + M_2 = \frac{4\pi^2 a^3}{GP^2}, \quad (7)$$

then, using the determined photometric solutions of mode 4, the absolute parameters can be estimated as follows:  $M_1 = 1.573 (\pm 0.044)M_\odot$ ,  $M_2 = 0.677 (\pm 0.082)M_\odot$ ,  $R_1 = 1.551 (\pm 0.002)R_\odot$ ,  $R_2 = 1.039 (\pm 0.002)R_\odot$ ,  $L_1 = 5.464 (\pm 0.394)L_\odot$ , and  $L_2 = 0.972 (\pm 0.003)L_\odot$ .

All available eclipse times were used to investigate the variations of the orbital period by analyzing the O–C diagram. The O–C analysis found that the period of TT Cet is decreasing at a rate of  $dP/dt = -5.01 (\pm 0.06) \times 10^{-8}$  d · yr<sup>-1</sup>. Such long-term period decrease may be the results of mass transfer from the primary component to the secondary one and the angular momentum loss (AML) from the binary system [e.g., Zhu et al. (2009), (2012), Liao et al. (2017), Liao, Qian, & Sarotsakulchai (2019)]. Case A mass transfer from primary to the secondary component occurs commonly in SD1-type semi-detached systems, such as BL And (Zhu & Qian 2006). The thermal timescale and nuclear timescale of the primary star are  $\tau_{th} = 2 \times 10^7 M_2^2 / L_2 R_2 = 9.08 \times 10^6$  yr and  $\tau_N = 10^{10} M_2 / L_2 = 6.97 \times 10^9$  yr, respectively. The timescale of period decrease is  $\tau_p = P/\dot{P} = 9.7 \times 10^6$  yrs, which is more close to the thermal timescale of the primary star. It means that the mass transfer in TT Cet is occurring on the thermal timescale of the primary star. Assuming the conservation of mass, the following equation can be used to calculate the rate of mass transfer:

$$\dot{P}/P = 3(1 - M_2/M_1) \cdot M_2/M_2. \quad (8)$$

This leads to  $\dot{M}_2/M_2 = 6.03 (\pm 0.12) \times 10^{-8}$  yr<sup>-1</sup>, and the timescale of mass transfer is  $\tau \sim M_2/\Delta M_2 \sim 1.67 \times 10^7$  yrs. We note that such a period change may also be one part of a cyclic variation



caused by the third body with a much longer period, such as 250 yr, while this possibility also needs more observation evidence.

Using the Kepler third law and the photometric solutions with mode 4, the mean densities of the primary and secondary star were calculated as  $\rho_1 = 0.420\rho_\odot$  and  $\rho_2 = 0.601\rho_\odot$ , respectively. The corresponding logarithm values are  $\log \rho_1/\rho_\odot = -0.377$  and  $\log \rho_2/\rho_\odot = -0.221$ . Compared with the main sequence stars with same spectra type (Cox & Pilachowski 2000), the mean densities of both components are quite lower, which indicates that the components may evolved away from the zero age main sequence (ZAMS) line.

The asymmetrical light curves of TT Cet show obvious brightness enhancement around the primary light maximum, which may be caused by the hot spot on the surface of the secondary component. Accretion stream caused by the long-term mass transfer from the primary star will emerge on the surface of the secondary component, and then it will move to one side of the midline of the two stars, which will lead to local brightness enhancement of the surface (Hilditch et al. 1997). The latitude and longitude of the spot centre are about  $85.81^\circ$  and  $100.56^\circ$ , and the angular radius of the spot is about  $22.6^\circ$ , which follow the law of hot spot distribution on the secondary component (Hilditch et al. 1998). Hot spot is one kind of vestige of mass transfer, so the area of hot spot can be regarded as an indirect measurable parameter of mass transfer. The proportion of hot spot area in the surface of the secondary component is about 3.16%. Moreover, the long-term orbital period decrease of TT Cet supports the mass transfer from the primary to the secondary and is consistent with its primary filling configuration, which is another evidence of the mass transfer between components.

Semi-detached systems with lobe filling primaries like TT Cet are particular targets lying on key evolutionary phases, which are quite rarely in observation. TT Cet maybe in the broken contact stage predicted by the thermal relaxation oscillations theory (TRO) (Lucy 1976; Flannery 1976; Robertson & Eggleton 1977; Lucy & Wilson 1979). The geometric structure of such semi-detached system with the primary filling the Roche lobe and the secondary nearly filling the Roche lobe is quite instability. However, such oscillation phase is quite short compared with the whole life times of the components. During the semi-detached phase, the light curves of such systems show classical EB-type characteristic. The orbit will shrink, and the period will decrease continuously because of the Case A mass transfer from the primary component to the secondary one. The period decrease and the semi-detached configuration with lobe filling primary reveal that TT Cet has reached the broken contact stage. Meanwhile, the AML via magnetic braking could also play a key role during the evolution process [e.g., Qian (2001) and (2003)]. With the period decrease, the secondary star will expand to fill the Roche lobe, then TT Cet will eventually evolve to the contact stage [e.g., Liao, Qian & Liu (2012) and Qian & Yang (2005)]. It is another good observational example supporting the TRO theory.

### 5.2. Preliminary statistic results of SD1-type NCBs

We collected all ascertained SD1-type NCBs from the literatures based on the tables of Zhu et al. (2009) and Zhu & Qian (2009). These systems were tabulated in Table 5. The light curves of SD1-type NCBs show enhanced brightness around the primary maximum commonly. The periods of the samples are all less than 1 d. The periods only show decrease variation, which indicates that

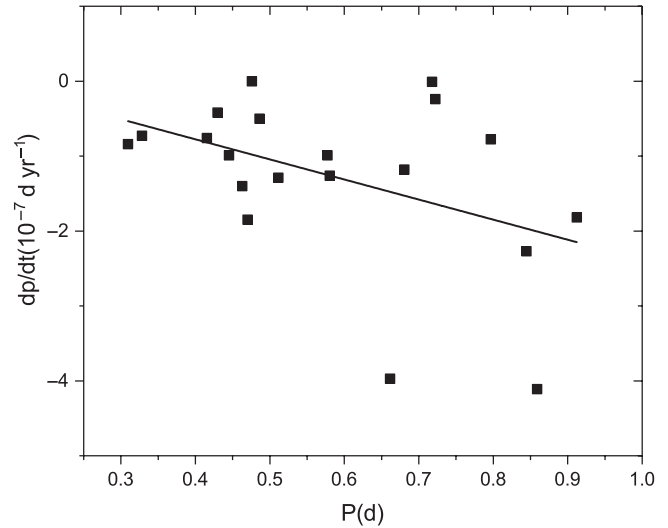


Figure 10. The  $dP/dt$ - $P$  relation of SD1-type NCBs.

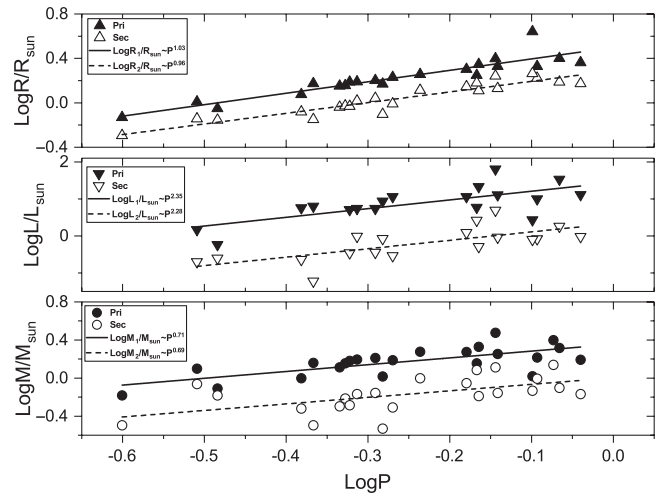


Figure 11. The R-P, L-P, and M-P relations of SD1-type NCBs.

the mass transfer may play an important role in the structural evolution process of these systems, which has been suggested by Zhu et al. (2009) and Zhu & Qian (2009).

The correlation of  $dP/dt$ - $P$  of SD1-type NCBs is shown in Figure 10, which is similar to the corresponding correlations of the SD2-type NCBs and the Algol semi-detached systems with decreasing periods (Zhu & Qian 2009). The function of the linear fit is  $dP/dt = 0.30(\pm 0.81) - 2.68(\pm 1.32)P$ . The radii-period (R-P, including  $R_1$ -P and  $R_2$ -P), luminosity-period (L-P, including  $L_1$ -P and  $L_2$ -P) and mass-period (M-P, including  $M_1$ -P and  $M_2$ -P) relations are plotted in Figure 11. The radii-mass (R-M) and luminosity-mass (L-M) relations are plotted in Figure 12. The corresponding relation equations are listed as follow, in which  $r$  represents the correlation coefficient,

$$\log R_1/R_\odot = 0.50(3) + 1.03(10) \log P (r = 0.83), \quad (9)$$

$$\log R_2/R_\odot = 0.29(2) + 0.96(8) \log P (r = 0.88), \quad (10)$$

$$\log L_1/L_\odot = 1.44(17) + 2.35(60) \log P (r = 0.46), \quad (11)$$

$$\log L_2/L_\odot = 0.34(16) + 2.28(58) \log P (r = 0.46), \quad (12)$$

**Table 5.** Parameters of SD1-type near-contact binaries

Star	Period (d)	$q(M_2/M_1)$	Enhancement phase	$T_1$ (K)	$T_2$ (K)	$M_1$ $M_\odot$	$M_2$ $M_\odot$	$R_1$ ( $R_\odot$ )	$R_2$ ( $R_\odot$ )	$L_1$ ( $L_\odot$ )	$L_2$ ( $L_\odot$ )	$dP/dt$ ( $10^{-7}d \cdot yr^{-1}$ )	Ref
BO Peg	0.58043	0.55	Uncertain	-	-	1.9	1.0	1.8	1.3	-	-	-1.26	(1)(2)
V1010 Oph	0.66144	0.470	Around 0.25	7 500	5 132	1.887	0.887	2.01	1.40	11.45	1.22	-3.97	(3)(4)
V361 Lyr	0.30961	0.694	0.17-0.46	6 200	4 500	1.26	0.87	1.02	0.72	1.48	0.20	-0.84	(5)(6)
BL And	0.72238	0.377	0.22-0.38	7 500	4 830	1.8	0.7	2.13	1.35	12.86	0.92	-0.24	(7)
V388 Cyg	0.85905	0.3653	0.05-0.50	8 750	5 543	2.08	0.79	2.52	1.54	33.88	1.82	-4.11	(8)(9)
RT Scl	0.51156	0.433	0.20-0.48	7 000	4 820	1.63	0.70	1.59	1.10	5.50	0.36	-1.29	(10)(11)
CN And	0.46279	0.3885	0.20-0.40	6 500	5 922	1.299	0.505	1.425	0.916	-	-	-1.40	(12)(13)
GR Tau	0.42985	0.2192	0.20-0.40	7 500	3 434	1.45	0.32	1.49	0.71	6.38	0.06	-0.42	(14)(15)
FT Lup	0.47008	0.465	0.10-0.40	6 700	3 916	1.43	0.61	1.43	0.94	-	-	-1.85	(16)
V473 Cas	0.41546	0.493	0.30-0.43	5 830	4 378	1	0.48	1.19	0.83	5.70	0.23	-0.76	(17)
BS Vul	0.47597	0.340	0.25-0.45	7 000	4 632	1.52	0.52	1.54	0.93	5.13	0.35	-0.0007	(18)
NP Aqr	0.80698	0.598	Uncertain	7 050	4 250	1.65	0.99	2.13	1.67	10	0.83	-	(19)
V609 Aql	0.79657	0.70	Uncertain	6 050	5 000	1.05	0.74	4.39	1.84	2.70	0.8	-0.775	(20)
DO Cas	0.68467	0.304	Uncertain	8 350	4 297	2.130	0.650	2.22	1.29	21.47	0.51	-	(4)(21)(22)
V747 Cen	0.53719	0.320	Around 0.25	8 150	4 275	1.541	0.493	1.70	0.98	11.42	0.29	-	(4)
VV Cet	0.52239	0.284	Uncertain	8 150	6 252	1.042	0.296	1.48	0.79	8.66	0.85	-	(4)
TT Her	0.91210	0.439	Uncertain	7 239	4 690	1.56	0.68	2.30	1.49	13.0	0.96	-1.82	(23)(24)
V1374 Tau	0.25086	0.48	0.60-0.90	4 100	3 455	0.66	0.32	0.742	0.508	-	-	-	(25)
GO Cyg	0.71776	0.428	Uncertain	10 350	6 490	3.0	1.3	2.50	1.75	64	4.9	-0.01	(26)
IR Cas	0.68069	0.851	Uncertain	6 750	5 992	1.43	1.22	1.77	1.51	5.85	2.63	-1.18	(27)
V369 Cep	0.32819	0.85	0.30-0.45	5 348	4 985	0.78	0.66	0.89	0.70	0.58	0.25	-0.73	(28)
V525 Sgr	0.70512	0.55	0.25-0.35	9 250	6 200	-	-	-	-	-	-	-	(29)
TT Cet	0.48595	0.43	0.10-0.40	7 091	5 414	1.57	0.68	1.55	1.04	5.46	0.97	-0.501	This study
DM Del	0.84468	0.550	Uncertain	8 770	4 823	2.51	1.38	-	-	-	-	-2.27	(30)
FF Vul	0.44499	0.4852	Around 0.25	6 500	4 958	-	-	-	-	-	-	-0.99	(31)
V530 And	0.57722	0.3786	Uncertain	7 000	6 500	-	-	-	-	-	-	-0.99	(32)

(1) = Yamasaki & Okazaki (1986); (2) = Qian (2002b); (3) = Lipari & Sisto (1987); (4) = Siwak, Zola, & Koziel-Wierzbowska (2010); (5) = Lister (2009); (6) = Hilditch et al. (1997); (7) = Zhu & Qian (2006); (8) = Kang et al. (2001); (9) = Oh et al. (1997); (10) = Duerbeck & Karimie (1979); (11) = Hilditch & King (1986); (12) = Van Hamme et al. (2001); (13) = Cai et al. (2019); (14) = Qian (2002a); (15) = Gu et al. (2004); (16) = Lipari & Sisto (1986); (17) = Zhu et al. (2009); (18) = Zhu et al. (2012); (19) = İbanoğlu, Çakırlı, & Dervişoğlu (2010); (20) = Turner et al. (2008); (21) = Liu, Zhang, & Zhang (1988); (22) = Jafarzadeh (2006); (23) = Milano et al. (1989); (24) = Terrell & Nelson (2014); (25) = Austin et al. (2011); (26) = Ulaş et al. (2012); (27) = Li et al. (2014); (28) = Zhu et al. (2014); (29) = Haans & Malasan (2019); (30) = He & Qian (2010); (31) = Samec et al. (2016); (32) = Samec et al. (2014).

$$\log M_1/M_\odot = 0.35(5) + 0.71(16) \log P(r = 0.47), \quad (13)$$

$$\log M_2/M_\odot = 0.003(64) + 0.69(22) \log P(r = 0.28), \quad (14)$$

$$\log R/R_\odot = 0.14(2) + 0.60(8) \log M/M_\odot (r = 0.59), \quad (15)$$

$$\log L/L_\odot = 0.33(5) + 2.71(24) \log M/M_\odot (r = 0.79). \quad (16)$$

The above relationships are very similar to that of NCBs acquired by Zhu et al. (2009) and Zhu & Qian (2009). We note that in Figure 11, there are two total absences of samples with periods around 0.35 and 0.5 d. The gap near 0.5 d may be caused by the selection effect of the samples apparently, because the binaries with period close to 12 h are difficult to observe. Such gap also appears in the relation of contact binaries (Gazetas & Niarchos 2006). While the gap near 0.35 d is very interesting, more observation data are needed to understand this feature. The radii, luminosity, and mass of components are correlated with the period of the system, which is shown obviously in Figure 11.

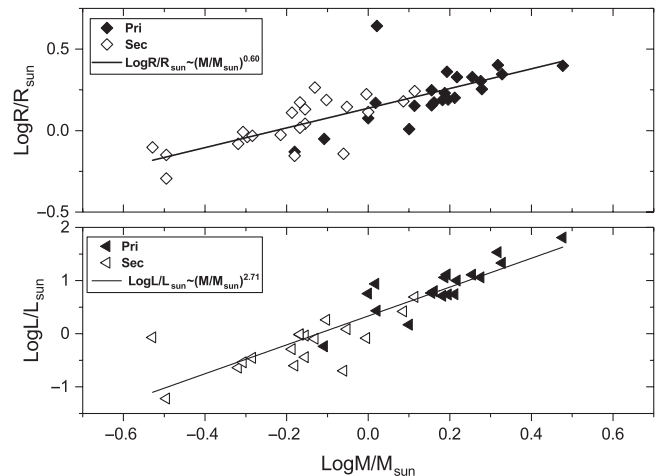


**Figure 12.** The R-M and L-M relations of SD1-type NCBs.

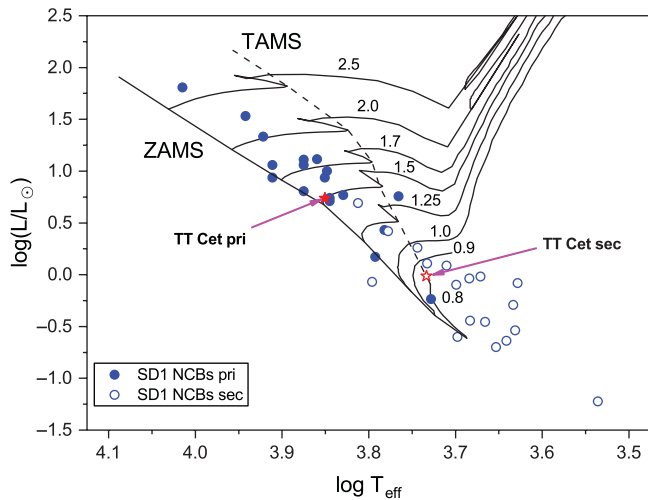


**Figure 13.** The temperature-luminosity diagram of SD1-type NCBs.

The correlation coefficient of the R–P relation is much larger than that of L–P and M–P relations. The coefficient of radii-mass relation and luminosity-mass relation are estimated as 0.60 and 2.71, respectively. The coefficient of R–M relation is larger than that of W Uma-type over-contact systems (0.46), but less than that of detached systems (0.724). Meanwhile, the coefficient of L–M relation is very near to that of the main sequence systems (2.76). The temperature-luminosity diagram of SD1-type NCBs including TT Cet is plotted in Figure 13. In the figure, the ZAMS and terminal-age main sequence lines are acquired by Schaller et al. (1992) at  $Z = 0.020$ . From the figure, we can see that the primary components of SD1-type NCBs are located in the main sequence, and the secondaries have evolved from the main sequence. The results indicate that the two components of SD1-type NCBs may lay in the similar evolutionary, and the secondary component has higher degree of evolution.

**Acknowledgements.** We are very appreciate and feel great thankful for the hard works on the fight to COVID-19 to the Chinese people and all the people worldwide. We would like to thank the editor and the referee very much for the very valuable and useful comments that help improved this paper. This work was partly supported by the National Natural Science Foundation of China (Nos. 11922306, U1631108, and U1831109) and CAS Interdisciplinary Innovation Team. We acknowledge the support of the staff of the Xinglong 2.16-m telescope. This work was partially supported by the Open Project Program of the Key Laboratory of Optical Astronomy, National Astronomical Observatories, Chinese Academy of Sciences.

CCD photometric observations of the system were obtained with the 1-m telescope administered by YNO and the 70-cm telescope at Lijiang station, YNO. The spectra observation were obtained with the 2.16-m telescope at Xinglong station of National Astronomical Observatory.

## References

Wilson, R. E., & Devinney, E. J. 1971, *ApJ*, 166, 605  
 Agerer, F., & Hubscher, J. 1999, *IBVS*, 4711  
 Agerer, F., & Hubscher, J. 2002, *IBVS*, 5296  
 Agerer, F., & Huebscher, J. 1998, *IBVS*, 4562, 1  
 Austin, S. J., Robertson, J. W., de Souza, T. R., Tycner, C., & Honeycutt, R. K. 2011, *AJ*, 141, 124  
 Ažusienis, A., & Straizys, V. 1969, *SvA*, 13, 316  
 Bessell, M. S. 1983, *PASP*, 95, 480

Brancewicz, H. K., & Dworak, T. Z. 1980, *AcA*, 30, 501  
 Cai, J.-T., Yu, Y.-X., Hu, K., & Xiang, F.-Y. 2019, *RAA*, 19, 106  
 Cakirli, O., Gungor, C., Pinar, A., & Camurdan, C. M., 2006 *IBVS*, 5729, 1  
 Cox, A. N., & Pilachowski, C. A. 2000, *PhT*, 53, 77  
 Deb, S., & Singh, H. P. 2011, *MNRAS*, 412, 1787  
 Diethelm, R. 2010, *IBVS*, 5920, 1  
 Diethelm, R. 2011, *IBVS*, 5960, 1  
 Diethelm, R. 2012, *IBVS*, 6011, 1  
 Diethelm, R., et al. 1974, *BBSAG*, 16, 1  
 Duerbeck, H. W., & Karimie, M. T. 1979, *IBVS*, 1617, 1  
 Duerbeck, H. W., & Rucinski, S. M. 2007, *AJ*, 133, 169  
 Fan, Z., et al. 2016, *PASP*, 128, 115005  
 Flannery, B. P. 1976, *ApJ*, 205, 217  
 Gaia Collaboration, et al. 2018, *A&A*, 616, A1  
 Gazeas, K. D., & Niarchos, P. G. 2006, *MNRAS*, 370, L29  
 Giuricin, G., Mardirossian, F., & Mezzetti, M. 1983, *A&AS*, 54, 211  
 Gu, S.-H., Chen, P.-S., Choy, Y.-K., Leung, K.-C., Chung, W.-K., & Poon, T.-S. 2004, *A&A*, 423, 607  
 Haans, G. K., & Malasan, H. L., 2019, in *Journal of Physics Conference Series*, 012050, [10.1088/1742-6596/1127/1/012050](https://doi.org/10.1088/1742-6596/1127/1/012050)  
 He, J.-J., & Qian, S.-B. 2010, *PASJ*, 62, 441  
 Hilditch, R. W., & King, D. J. 1986, *MNRAS*, 223, 581  
 Hilditch, R. W., Collier Cameron, A., Hill, G., Bell, S. A., & Harries, T. J., 1997, *MNRAS*, 291, 749  
 Hilditch, R. W., Bell, S. A., Hill, G., & Harries, T. J. 1998, *MNRAS*, 296, 100  
 Hoffman, D. I., Harrison, T. E., Coughlin, J. L., McNamara, B. J., Holtzman, J. A., Taylor, G. E., & Vestrand, W. T. 2008, *AJ*, 136, 1067  
 Høg, E., et al. 2000, *A&A*, 355, L27  
 Hubscher, J., Steinbach, H.-M., & Walter, F. 2009, *IBVS*, 5889, 1  
 İbanoglu, C., çakırlı, Ö., & Dervişoğlu, A. 2010, *NewA*, 15, 373  
 Jafarzadeh, S. 2006, arXiv e-prints, [pp astro-ph/0610647](https://arxiv.org/abs/astro-ph/0610647)  
 Kang, Y. W., Kim, H.-I., Lee, W.-B., & Oh, K.-D. 2001, *MNRAS*, 325, 707  
 Kizilirmak, A., & Pohl, E. 1971, *IBVS*, 530, 1  
 Koleva, M., Prugniel, P., Bouchard, A., & Wu, Y. 2009, *A&A*, 501, 1269  
 Li, K., Hu, S. M., Guo, D. F., Jiang, Y. G., Gao, D. Y., & Chen, X. 2014, *AJ*, 148, 96  
 Liao, W. P., Qian, S. B., & Liu, N. P. 2012, *AJ*, 144, 178  
 Liao, W. P., Qian, S. B., Li, L. J., Zhou, X., Zhao, E. G., & Zhang, J. 2017, *PASP*, 129, 034201  
 Liao, W. P., Qian, S. B., & Sarotsakulchai, T. 2019, *AJ*, 157, 207  
 Lipari, S. L., & Sistero, R. F. 1986, *MNRAS*, 220, 883  
 Lipari, S. L., & Sistero, R. F. 1987, *AJ*, 94, 792  
 Lister, T. A. 2009, in *15th Cambridge Workshop on Cool Stars, Stellar Systems, and the Sun*, American Institute of Physics Conference Series, ed. E. Stempels (Vol. 1094), 688–691, doi: [10.1063/1.3099207](https://doi.org/10.1063/1.3099207)  
 Liu, Q.-Y., Zhang, Y.-L., & Zhang, Z.-S. 1988, *ChA&A*, 12, 216  
 Lucy, L. B. 1976, *ApJ*, 205, 208  
 Lucy, L. B., & Wilson, R. E. 1979, *ApJ*, 231, 502  
 Milano, L., Barone, F., Mancuso, S., Russo, G., & Vittone, A. A. 1989, *A&A*, 210, 181  
 Ogloza, W., Niewiadomski, W., Barnacka, A., Biskup, M., Malek, K., & Sokolowski, M. 2008, *IBVS*, 5843, 1  
 Oh, K.-D., Kim, H.-I., & Lee, W.-B. 1997, *Journal of Astronomy and Space Sciences*, 14, 33  
 Paschke, A. 2013, *OEJV*, 155, 1  
 Pribulla, T., et al. 2009, *AJ*, 137, 3655  
 Prugniel, P., & Soubiran, C. 2001, *A&A*, 369, 1048  
 Qian, S. 2001, *MNRAS*, 328, 635  
 Qian, S. 2002a, *MNRAS*, 336, 1247  
 Qian, S. 2002b, *A&A*, 387, 903  
 Qian, S. 2003, *MNRAS*, 342, 1260  
 Qian, S., & Yang, Y. 2005, *MNRAS*, 356, 765  
 Qian, S.-B., He, J.-J., Zhang, J., Zhu, L.-Y., Shi, X.-D., Zhao, E.-G., & Zhou, X. 2017, *RAA*, 17, 087  
 Qian, S. B., Zhang, J., He, J. J., Zhu, L. Y., Zhao, E. G., Shi, X. D., Zhou, X., & Han, Z. T. 2018, *ApJS*, 235, 5  
 Qian, S.-B., et al. 2019, *RAA*, 19, 064

- Robertson, J. A., & Eggleton, P. P. 1977, *MNRAS*, **179**, 359
- Ruciński, S. M. 1969, *AcA*, **19**, 245
- Samec, R. G., Kring, J., Flaaten, D., Faulkner, D. R., & Van, HAMME W. V. 2014, in *American Astronomical Society Meeting Abstracts #223*, 155.12
- Samec, R. G., Nyaude, R., Caton, D., & Van Hamme, W. 2016, *AJ*, **152**, 199
- Samolyk, G. 2008a, *JAVSO*, **36**, 171
- Samolyk, G. 2008b, *JAVSO*, **36**, 186
- Samolyk, G. 2010, *JAVSO*, **38**, 183
- Samolyk, G. 2011, *JAVSO*, **39**, 177
- Samolyk, G. 2012, *JAVSO*, **40**, 975
- Samolyk, G. 2013a, *JAVSO*, **41**, 122
- Samolyk, G. 2013b, *JAVSO*, **41**, 328
- Schaller, G., Schaerer, D., Meynet, G., & Maeder, A., 1992, *A&AS*, **96**, 269
- Shaw, J. S. 1994, *MmSAI*, **65**, 95
- Siwak, M., Zola, S., & Koziel-Wierzbowska, D. 2010, *AcA*, **60**, 305
- Terrell, D., & Nelson, R. H. 2014, *ApJ*, **783**, 35
- Turner, D. G., Panko, E. A., Sergienko, O., Lane, D. J., & Majaess, D. J. 2008, *Obs*, **128**, 2
- Ulaş, B., Kalomeni, B., Keskin, V., Köse, O., & Yakut, K. 2012, *NewA*, **17**, 296
- Van Hamme, W., Samec, R. G., Gothard, N. W., Wilson, R. E., Faulkner, D. R., & Branly, R. M. 2001, *AJ*, **122**, 3436
- Vanden Berk, D. E., et al. 2001, *AJ*, **122**, 549
- Wilson, R. E. 1990, *ApJ*, 356, 613
- Wilson, R. E. 2012, *AJ*, 144, 73
- Wolf, G. W., & Kern, J. T. 1983, *ApJS*, **52**, 429
- Yamasaki, A., & Okazaki, A. 1986, *PASP*, **98**, 1325
- Zhu, L., & Qian, S. 2006, *MNRAS*, **367**, 423
- Zhu, L., & Qian, S. 2009, in Murphy S. J., Bessell M. S., eds, *Astronomical Society of the Pacific Conference Series Vol. 404, The Eighth Pacific Rim Conference on Stellar Astrophysics: A Tribute to Kam-Ching Leung*. p. 189
- Zhu, L. Y., Qian, S. B., Zola, S., & Kreiner, J. M. 2009, *AJ*, **137**, 3574
- Zhu, L. Y., Zejda, M., Mikulášek, Z., Liška, J., Qian, S. B., & de Villiers, S. N. 2012, *AJ*, **144**, 37
- Zhu, L. Y., et al. 2014, *AJ*, **147**, 42
- van Hamme, W. 1993, *AJ*, **106**, 2096